Shared subcortical arousal systems across sensory modalities during transient modulation of attention

Aya Khalaf[1], Erick Lopez[1], Jian Li[2,3], Andreas Horn[2,4,5,6], Brian L. Edlow[2,3], Hal Blumenfeld[1,7,8]

[1] Department of Neurology, Yale University School of Medicine, New Haven, CT, USA

[2] Center for Neurotechnology and Neurorecovery, Department of Neurology, Massachusetts General Hospital and Harvard Medical School, Boston, MA, USA

[3] Athinoula A. Martinos Center for Biomedical Imaging, Massachusetts General Hospital and Harvard Medical School, Charlestown, MA, USA

[4] Center for Brain Circuit Therapeutics, Department of Neurology, Brigham & Women's Hospital and Harvard Medical School, Boston, MA, USA

[5] Department of Neurosurgery, Massachusetts General Hospital and Harvard Medical School, Boston, MA, USA

[6] Movement Disorders & Neuromodulation Section, Department of Neurology, Charité – Universitätsmedizin, Berlin, Germany

[7] Department of Neuroscience, Yale University School of Medicine, New Haven, CT, USA

[8] Department of Neurosurgery, Yale University School of Medicine, New Haven, CT, USA

Correspondence to: Hal Blumenfeld, MD, PhD
Yale Depts. Neurology, Neuroscience, Neurosurgery
333 Cedar Street, New Haven, CT 06520-8018
Tel: 203 785-3865 Fax: 203 737-2538
Email: hal.blumenfeld@yale.edu

Key words: Attention Modulation, Arousal, Consciousness, Subcortical Networks, fMRI

Running title: Shared subcortical arousal systems

Abstract (150 words)

Subcortical arousal systems are known to play a key role in controlling sustained changes in attention and conscious awareness. Recent studies indicate that these systems have a major influence on short-term dynamic modulation of visual attention, but their role across sensory modalities is not fully understood. In this study, we investigated shared subcortical arousal systems across sensory modalities during transient changes in attention using block and event-related fMRI paradigms. We analyzed massive publicly available fMRI datasets collected while 1,561 participants performed visual, auditory, tactile, and taste perception tasks. Our analyses revealed a shared circuit of subcortical arousal systems exhibiting early transient increases in activity in midbrain reticular formation and central thalamus across perceptual modalities, as well as less consistent increases in pons, hypothalamus, basal forebrain, and basal ganglia. Identifying these networks is critical for understanding mechanisms of normal attention and consciousness and may help facilitate subcortical targeting for therapeutic neuromodulation.

Introduction

Different sensory modalities elicit distinct neural signatures in the brain. However, it is reasonable to assume that there is a fundamental subset of circuits shared across modalities, supporting core functions such as conscious perception and attention control. Subcortical arousal

systems are known to play a key role in controlling sustained changes of attention and long-lasting states such as sleep/wake and levels of vigilance[1]. Previous studies on patients with disorders of consciousness confirmed the critical influence of subcortical arousal systems in maintaining states of consciousness[2-4]. However, the role of these subcortical systems in dynamic modulation of attention has been less studied and when examined, the focus has often been on a single sensory modality without considering the shared networks dynamically modulating attention across perceptual modalities[5-7]. Moreover, most research investigating dynamic changes in attention has focused on cortical large-scale networks involved in top-down attentional salience and bottom-up attention control with little emphasis on subcortical systems[8-11].

Subcortical systems have been increasingly recognized as playing an important role in cognition[12]. Studies on healthy participants and patients with impaired consciousness have demonstrated that the midbrain reticular formation and central thalamus are key subcortical structures that modulate attention[2-4, 13-17]. Additionally, deep brain stimulation studies in humans and animal models demonstrated that stimulation of the central thalamus significantly improves arousal and restores consciousness[18-22]. Previous research suggests that arousal systems in the thalamus, upper brainstem and basal forebrain may contribute to dynamic modulation of attention and conscious perception[5, 6, 23-25]. The dynamic modulation of attention by the subcortical arousal systems is a key mechanism that facilitates conscious perception. Previously, we introduced a data-driven model that describes the sequence of neural mechanisms required to produce conscious awareness[26]. The model hypothesizes that one of the mechanisms critical for conscious perception is an attention mechanism that operates through cortical and subcortical arousal systems, mediating stimulus detection, dynamic modulation of arousal, bottom-up

attentional salience, and top-down attentional control. In this framework, the subcortical arousal networks provide an early dynamic transient pulse that facilitates subsequent widespread signals necessary for conscious perception[26]. While multiple cortical systems have been implicated in attention and conscious perception[27], the potential key role of subcortical arousal networks in modulating attention and perception across sensory modalities requires further investigation.

Functional magnetic resonance imaging (fMRI) experiments typically use block designs, event-related designs, or a combination of both to identify and characterize both sustained and transient blood-oxygenation level-dependent (BOLD) responses[28-32]. Previous studies have noted cortical BOLD fMRI signal increases at the onset and offset of blocks and events[33-35], with a few studies investigating BOLD fMRI signal increases in subcortical networks at the onset of blocks and events[6, 7, 15]. Further research is needed to explore the shared subcortical networks facilitating these sustained and transient attention modulations at block onsets and in response to individual event stimuli, respectively.

In this study, we investigate the role of the subcortical arousal systems in dynamic modulation of attention across sensory modalities with large sample sizes using both block and event-related fMRI designs. Previous studies have highlighted the early transient signals in subcortical arousal systems, suggesting that a model-free fMRI analysis may be more effective at detecting these signals compared to traditional general linear models, which may not adequately capture such early responses[6, 7, 36, 37]. Therefore, we conducted a model-free fMRI analysis for each task included in the study by calculating percentage change in BOLD fMRI signals to identify the subcortical regions activated at task block onsets or in response to individual events, depending

on the task design. A conjunction analysis was performed to identify the subcortical regions sharing common early activity across different tasks and sensory modalities. Similarly, we performed a conjunction analysis to identify the shared cortical networks across sensory modalities. Our findings revealed a shared early transient surge in fMRI activity within subcortical arousal systems. Furthermore, we observed similar patterns in the cortical salience and attention networks. These findings provide new insights into brain mechanisms of arousal and attention and may help identify potential therapeutic targets for restoring arousal and consciousness in patients with neurological disorders.

Methods

Participants and behavioral tasks

We analyzed 3 Tesla (3T) task fMRI data collected from healthy adults while performing 11 different tasks spanning four sensory modalities: vision, audition, taste, and touch. The data were obtained from six publicly available datasets, providing a large overall sample size (Table 1). The datasets included were the WU-Minn Human Connectome Project (HCP) Young Adult [38, 39], UCLA Consortium for Neuropsychiatric Phenomics[40], Glasgow University[41], Jagiellonian University[42], and two datasets from Yale University[43, 44]. The HCP dataset provided a significant portion of our data; specifically, task-fMRI data from the HCP 1200 Subjects Data Release were used in this study (N= 1113; mean age = 28.8; age range: 22–37 years; females = 606)[45]. In the visual domain, we examined six tasks, including, the gambling[46], relational processing[47], working memory[48, 49], social cognition[50], and motor[51] tasks from the HCP dataset as well as the spatial capacity task (SCAP)[40] from the UCLA Consortium (N=130; mean age ± SD = 31.26 ±

8.74 years; age range = 21-50 years; females = 62). For auditory tasks, we analyzed the language task[52] from the HCP dataset and the passive listening task [41] from the Glasgow University dataset (N = 218; mean age ± SD = 24.1 ± 7.0 years; age range = NA; females =101). As for the taste modality, fMRI data from two tasks[43, 44] collected at Yale University were incorporated in the analysis (N = 28; mean age ± SD = 27.14 ± 4.75 years; age range = 18–37 years; females = 20, and N=48; mean age ± SD = 27.71 ± 3.94 years; age range = 23-39 years; females = 29). Lastly, in the tactile modality, we analyzed fMRI data of a tactile task[42] collected at the Jagiellonian University (N=25; mean age ± SD= 25.68 ± 3.3 years; age range = 22-32 years; females = 25). Additional details about the behavioral tasks, fMRI acquisition parameters, and data used in the analysis can be found in the Supplementary Information. The purpose of including different tasks from multiple sensory modalities with large sample sizes is to provide a robust basis for our analyses, allowing identification of shared subcortical arousal systems irrespective of sensory modality, presented stimuli, or task demands.

Depending on the task-design, we analyzed fMRI data either at task block onset to investigate subcortical and cortical networks modulating transitions from baseline blocks to task blocks (block transitions), or at event onset to investigate networks modulating transitions from baseline to events (event transitions). Event transitions were specifically considered for analysis when the time between consecutive events was jittered, while block transitions were examined when a task block was preceded by a baseline block. These criteria led to the analysis of block transitions in nine tasks and event transitions in two tasks (Table 1). Information on the number of baseline blocks, task blocks, events, and the number of blocks/events used in the analysis is reported in Table 1. Note that in some cases the number of task blocks analyzed per run was fewer than the

number of task blocks per run. This was because we only analyzed task blocks that were preceded by a baseline block (baseline to task transitions), and for some run designs the first task block had no preceding baseline block, while in others, several task blocks were presented sequentially without baseline blocks separating them. More detailed descriptions of the tasks and fMRI data acquisition parameters are reported in the Supplementary Information.

Preprocessing and artifact rejection

A standard fMRI data preprocessing pipeline was implemented using the Statistical Parametric Mapping (SPM12) toolbox (http://www.fil.ion.ucl.ac.uk/SPM) in MATLAB (Mathworks, Inc.). This pipeline was applied to all tasks except those from the HCP dataset. The pipeline comprises three main steps, including motion correction, nonlinear spatial normalization to the standard Montreal Neurological Institute (MNI) space, and spatial smoothing with a Gaussian kernel. For motion correction, functional images acquired in each run were spatially realigned to the first image in that run using 3D rigid-body transformation with three translation and three rotation parameters in x, y, and z directions. To transform the motion-corrected functional images to the MNI space, the structural scan for each participant was coregistered to the mean functional image of the motion-corrected functional images within each run. Next, that structural scan was transformed by non-linear warping to the MNI space and the corresponding transformation matrix was applied to the motion-corrected functional images. Finally, the normalized functional images were spatially smoothed with an isotropic Gaussian kernel (FWHM = 6mm). Because the tactile task had a long repetition time (TR) of 3 seconds, we applied slice-timing correction in SPM12 before the standard preprocessing steps.

To ensure computational feasibility, we utilized the preprocessed version of the HCP data that had undergone minimal processing using the HCP pipelines[53]. The primary preprocessing steps for the HCP data aligned with the standard pipeline we implemented, with one main difference: the HCP pipeline included additional corrections for susceptibility distortions. These corrections required acquisition of field mapping scans, which were not available for the non-HCP datasets, rendering this step infeasible to replicate. Because the preprocessed HCP data were unsmoothed, we applied the Gaussian smoothing step (FWHM = 6mm) from our standard pipeline to maintain consistency with the non-HCP datasets.

For both HCP and non-HCP tasks, runs were excluded from the analysis if transient head movement exceeded 2 mm of translation and 1° of rotation in any of the three directions. These criteria resulted in excluding 2506 runs out of 13643 runs (18.37%) from the analysis. Information on excluded runs per task are reported in the Supplementary Information (Suppl Table S1). To further remove spatial and temporal noise from the data, the smoothed BOLD functional images were next passed through a five step denoising procedure as in previous work from our group[6, 7, 37]. Data were (1) grey matter masked to exclude non-grey matter voxels using a mask created based on a standard gray matter mask from MarsBaR (http://marsbar.sourceforge.net/) and modified to include the midbrain and pons (The mask volume in the MNI space will be publicly available upon publication here: https://github.com/BlumenfeldLab/Khalaf-et-al_2024), (2) filtered using a 1/128 Hz high-pass filter, (3) corrected for motion artifacts by utilizing a general linear model with the six rigid-body motion parameters estimated during functional image realignment to regress out motion, (4) subjected to rejection of individual volumes if the volume-to-volume root mean squared

difference in BOLD signal (DVARS) at certain time point exceeded a threshold of 5[54, 55], and (5) subjected to rejection of individual volumes if instantaneous changes in head position, known as framewise displacement (FD) exceeded a threshold of 0.3 at a certain time point[54, 55]. FD is calculated as the sum of the absolute values of change in head movement among the six rigid-body motion parameters.

Percent Change Analysis

To identify the subcortical and cortical networks showing transient BOLD changes at block and event onset, we performed a model-free fMRI analysis by calculating the percent change in BOLD signal across time for the whole brain[6, 7, 56]. Through the percent change analysis, we obtained percent change brain maps and percent change time courses showing the transient BOLD changes associated with block and event transitions. The tasks included in the analysis utilized four different TR values, including, 0.72 seconds (6 HCP tasks), 1 second (2 Yale tasks), 2 seconds (2 Glasgow and UCLA tasks), and 3 seconds for the tactile task. Percentage change analyses were conducted using the original TRs at which the tasks were acquired. All analyses were completed in MATLAB using custom functions as well as functions from SPM12.

Percent Change Brain Maps

The BOLD percent change was calculated for the time course of each voxel relative to the mean BOLD signal of that voxel across the entire run. The BOLD volume corresponding to the onset of a specific block/event was defined as the volume that immediately preceded the block/event onset. A block/event epoch included all volumes corresponding to the 15 seconds before the block/event onset to the 15 seconds after. Epochs were averaged across blocks/events within the same run then across runs, resulting in a single 30-second-long average percent change epoch for

each subject. Spatiotemporal cluster-based permutation testing was applied to these averaged epochs across subjects to identify the statistically significant voxels and time points compared to the baseline before the block/event onset (see Statistical Analysis section below).

Anatomical Localization and Percent Change Time Courses

To precisely localize the observed subcortical activity on the structural MRI template, we used several published *a priori* anatomical atlases. We used the Harvard ascending arousal network (AAN) atlas[57] for brainstem nuclei, the Morel atlas[58] for thalamic nuclei, the BGHAT atlas[59] for basal ganglia, as well as an atlas of basal forebrain and hypothalamus nuclei[60]. For the amygdala, we used the amygdala ROI available through the MNI PD25 atlas[61]. In addition to anatomical localization, we used the anatomical atlases to define ROIs for time course analysis in two regions showing shared changes across all modalities, represented by the midbrain reticular formation (AAN atlas) and the thalamic intralaminar central lateral nucleus (Morel atlas). To obtain the time-course of each ROI per subject, we averaged the percentage change time courses across voxels within that ROI using the data from the subject-level percent change maps (see *Percent Change Brain Maps* section). To identify the statistically significant time points compared to the baseline before the block/event onset, temporal cluster-based permutation testing was applied to the ROI time courses across subjects as described in the temporal analysis portion of the next section.

Statistical Analysis

We first performed separate statistical analyses for each of the 11 tasks in each modality, and then performed conjunction and disjunction analyses across sensory modalities. Spatiotemporal

cluster-based permutation testing was employed to identify voxels and time points showing statistically significant changes in post block/event percent change signals compared to the baseline prior to block/event onset[7]. This approach overcomes the multiple comparisons problem through calculating a single test statistic for the entire spatiotemporal percent change data grid instead of evaluating the statistical significance at each voxel-time point pair[62]. No assumptions are made about the hemodynamic response time course, thus avoiding problems where time course models may not fit the data in some brain regions[36, 37, 63]. Additionally, this nonparametric approach does not have assumptions about the distribution of the data which limits false positive rates, especially in high-dimensional data such as fMRI, unlike parametric methods that may incorrectly model functional MRI data, leading to higher false positive rates than their nominal rates[64]. The cluster-based permutation statistical approach implemented in this study was adapted from the Mass Univariate ERP Toolbox [65] in MATLAB.

Spatiotemporal Analyses

Spatiotemporal statistical analysis was conducted using the original TRs at which the tasks were acquired, except for the tactile task, for which the percentage change data were upsampled to a TR of 2 seconds prior to statistical analysis. The upsampling was achieved through applying linear interpolation to the subject-level percentage change epochs. This was performed as part of our procedure to standardize our analysis TR across all tasks, allowing for the statistical analysis outcomes to be temporally aligned across tasks to enable identification of shared and unique subcortical and cortical regions across time through application of conjunction and disjunction analyses (see Subcortical and Whole-brain Conjunction and Disjunction Analyses section for more details on common TR selection across tasks). Given the high dimensionality of fMRI data, to improve computational efficiency we implemented two versions of our statistical analysis[7]; a

high-resolution version to identify statistically significant changes in subcortical areas, as well as a lower-resolution version to identify statistically significant changes in the whole brain. In the high-resolution subcortical statistical analysis, the spatial resolution of the data was preserved at 2 mm isotropic, but to speed processing the voxels included in the analysis were restricted to the subcortical grey matter voxels in the brainstem, thalamus, basal ganglia, basal forebrain and hypothalamus. In the lower-resolution whole-brain analysis, all the voxels in the grey matter were included, adding the cerebral cortex and cerebellum, but reducing the spatial resolution of the data from 2x2x2 to 6x6x6 mm^3 to improve computational efficiency. Both the high-resolution subcortical and low-resolution whole-brain statistical analyses were applied to the percent change epochs across subjects in a given task to identify the statistically significant voxels and time points post block/event onset compared to the baseline before the block/event onset. The baseline was defined as the 6 seconds prior to block/event onset.

For the whole brain analysis, spatial resolution was reduced by combining spatially adjacent 2x2x2 mm^3 grey matter voxels to form larger 6x6x6 mm^3 voxels. Specifically, the central voxels for each of the 6x6x6 mm3 lower-resolution voxels were defined as the original 2x2x2 mm^3 voxels positioned with exactly 2 intervening voxels until the next central voxel in the x, y, and z directions. Next, all adjacent voxels sharing a face, edge, or vertex with a central voxel were found. These adjacent voxels combined with the central voxel formed the 6x6x6 mm^3 voxel. Finally, the BOLD percent change signal value within each of the lower spatial resolution 6x6x6 mm^3 voxels was determined by computing the mean BOLD signal across all 2x2x2 mm^3 voxels within each of the lower resolution 6mm3 voxels. If all the adjacent voxels for a certain central voxel were located in the grey matter, the 6x6x6 mm^3 voxel would include 27 (33) of the 2x2x2

mm^3 voxels. Otherwise, the larger voxel would combine all available adjacent voxels resulting in a non-cuboidal shaped voxel.

Cluster-based spatiotemporal permutation analysis was performed by generating the spatiotemporal cluster null distribution through 5000 permutation iterations. For each permutation, the mean of the 6-second percent change baseline at a specific voxel and the percent change value of that voxel at the tested time point were randomly shuffled based on the direction of subtraction (time point minus baseline or baseline minus time point) for each participant. Next, a paired, two-tailed t-test compared the permuted values across participants to identify the statistically significant voxels at each tested time point ($p < 0.05$) from -15 seconds before block/event onset up to 15 seconds afterwards.) Statistically significant spatiotemporal clusters were formed by considering spatial and temporal adjacencies. Negative and positive clusters were created independently. Spatially adjacent voxels were defined as statistically significant voxels (in the same direction) sharing a face, edge, or vertex. Temporal adjacency was found if a voxel was statistically significant (in the same direction) at two or more sequential time points. For each spatiotemporal cluster, the summed absolute value of t-values was computed across all voxels and time points belonging to that cluster. The largest negative and positive cluster determined separately by summed absolute value of t-values was selected from each permutation. Because the positive and negative values were randomly shuffled, we assumed symmetry in the permutation distribution, so we only retained negative clusters and created a one-sided distribution to reduce computations. Therefore, the p-value threshold was set at 0.025 (equivalent to 0.05 in a two-sided distribution). For each permutation, we retained only the negative cluster with the largest absolute t-value and collected these values across 5000

permutations to create a permutation distribution. After generating the spatiotemporal cluster null distribution, the spatiotemporal cluster forming analysis described above was applied to the unpermuted data. Positive and negative clusters were identified separately, and summed t-values with absolute value above the top 2.5% of the permutation distribution were considered significant.

The cluster-based spatiotemporal analysis was performed separately on the whole brain at 6x6x6 mm^3 resolution, and on subcortical regions at 2x2x2 mm^3 resolution. Importantly, the high resolution 2x2x2 mm^3 analysis improved the spatial identification of small subcortical regions, but did not add any new regions to the final conjunction analysis results that were not seen in the whole brain lower resolution analysis. Therefore, for display purposes when showing results of whole brain 6x6x6 mm^3 resolution analysis on cortical brain slices, we superimposed the 2x2x2 mm^3 resolution results for subcortical structures on the same slices/surfaces (e.g. Figures 3, 5 and Supplementary Presentations S1 – S3).

Temporal Analyses

We implemented a temporal cluster-based permutation test, which is an adapted version of the spatiotemporal cluster-based permutation test described above to identify the statistically significant changes in the ROI percent change time courses[7]. In particular, the cluster-forming approach in the temporal analysis considered only temporal adjacency unlike the spatiotemporal version, which considers both spatial and temporal adjacencies to form spatiotemporal clusters. For each ROI, the temporal cluster-based permutation test was applied to the percent change time courses across subjects for a given task to identify the statistically significant time points

post block/event onset compared to the baseline before the block/event. The baseline was defined as the 6 seconds prior to block/event onset. Before applying temporal statistical analysis, percentage change data for all tasks were resampled to a common TR as part of our procedure to standardize our analysis TR across all tasks, allowing for the statistical analysis outcomes to be temporally aligned to enable identification of shared ROIs and time points modulating transient changes of attention. Subject-level percentage change epochs per task were upsampled through applying linear interpolation. To improve time course visualization, we selected a common TR of 0.72 seconds (HCP sampling rate) for upsampling which represents the smallest TR across the datasets included in the study.

Subcortical and Whole-brain Conjunction and Disjunction Analyses

Binary Conjunction Analysis

To identify the shared subcortical and cortical networks across tasks and sensory modalities, we performed a binary conjunction analysis at each of the time points within an epoch (15 seconds pre and post block/event onset) across tasks. We refer to this as binary conjunction because a voxel was either included or not in the results based on all-or-none statistical criteria. For a voxel to be included in this conjunction, it had to show statistically significant changes (based on permutation testing) in the same direction (i.e., positive or negative) across all modalities and across all 11 tasks at the same time point. Voxels with both positive and negative changes at a given time point were not included in the binary conjunction brain maps. The binary conjunction analysis was performed separately for the high-resolution subcortical and lower-resolution whole-brain statistical results from the permutation testing.

Before applying the conjunction analysis, a procedure to standardize the analysis TR was developed to ensure the volumes subjected to the analysis are temporally aligned at each time point. Although the epoch length was 30 seconds for all tasks, the epoch length in volumes varied depending on the TR used for the fMRI data acquisition. Since the conjunction analysis had to be performed at the same time points across tasks, epochs from all tasks had to be resampled with the same TR. As mentioned earlier, the tasks included in the analysis utilized four different TR values, including, 0.72 seconds (6 HCP tasks), 1 second (2 Yale tasks), 2 seconds (2 Glasgow and UCLA tasks), and 3 seconds for the tactile task. To minimize the need for upsampling epochs and creation of new data points that were not physically acquired in the scanner, we selected a common TR of 2 seconds. With this TR, only the tactile task had to be upsampled from TR=3 seconds to TR=2 seconds. Specifically, the upsampling was performed on the subject-level percentage change epochs using linear interpolation. Cluster-based permutation statistics were applied to the resampled epochs as described above (see Statistical Analysis section) to identify the statistically significant voxels and time points. The HCP tasks, acquired with a TR of 0.72 seconds, were downsampled to TR=2 seconds through nearest neighbor interpolation to avoid introducing new data points while the Yale taste perception tasks, collected at a TR of 1 second, were downsampled by skipping every other volume. Cluster-based permutation statistics were applied to the HCP, Yale, Glasgow, and UCLA tasks at their original acquisition TRs.

Graded Conjunction Analysis

The binary conjunction approach had strict inclusion criteria, meaning a region would only be included in the conjunction if it was significant across all sensory modalities and tasks at the

same time points. To identify regions that are statistically significant across most sensory modalities but not all of them, we introduced a graded conjunction method, to identify significant voxels in 1, 2, 3 or all 4 modalities. Initially, binary conjunctions were conducted within each sensory modality to identify voxels sharing increases or decreases at the same time point, using the same binary approach already described. This process yielded binary maps for statistically significant increases or decreases across tasks for each sensory modality. Subsequently, these maps were aggregated separately for increases and decreases, with voxel values indicating the number (1 to 4) of sensory modalities sharing statistically significant changes in the same direction (i.e., positive or negative) at each time point. Note that for the tactile modality, it was not possible to perform conjunction analysis within modality since there was only one tactile task included in the study. Instead, we binarized the statistical significance maps of the tactile task at each time point and combined them with the binary conjunction maps from the other modalities to form the graded conjunction maps.

To provide a detailed description of the subcortical graded conjunction maps and the specific involvement of subcortical ROIs for each sensory modality and across modalities, we visually examined the binary conjunction maps for each modality at all the subcortical ROIs included in the study. Each ROI was assessed to determine whether it predominantly overlapped with increases or decreases in the binary conjunction maps. Regions where more than 50% of the ROI overlapped with significant changes were identified per modality. Number of modalities sharing increases or decreases per ROI were reported.

Disjunction Analyses

We performed exclusive disjunction analyses to identify subcortical and cortical regions unique for each sensory modality. Similar to the conjunction analyses, we performed the disjunction

analyses separately on the high-resolution subcortical and lower-resolution whole-brain statistical maps. We first obtained binary conjunction maps across tasks within each sensory modality to identify voxels sharing increases or decreases at the same time point, as already described. We then performed disjunction analysis comparing each modality to the other three. For a voxel to be included in the disjunction of a specific sensory modality, it had to show statistically significant changes in a specific direction (i.e., positive or negative) only in the binary conjunction maps of that sensory modality but not in the binary conjunction maps of any of the other three modalities at the same time point.

Brain Map Visualization

The conjunction and disjunction maps we obtained were overlaid on a 100 micron 7T MRI structural scan of an ex vivo human brain[66] for improved visualization and localization of the subcortical structures of interest. These maps were also plotted on the fsaverage FreeSurfer (https://surfer.nmr.mgh.harvard.edu/) inflated brain surface (left hemisphere: lh.inflated surface; right hemisphere: rh.inflated surface) to show the spatial extent of the shared cortical networks as well as the cortical networks unique to each sensory modality.

Time-Course Conjunction Analysis

We performed a binary conjunction analysis on the ROI time courses to identify the time points sharing common significant changes across all modalities and tasks relative to the baseline before block/event onset for each subcortical ROI. Similar to the conjunction analysis applied to brain maps, for a time point to be included in the conjunction, it had to show statistically significant changes in the same direction (i.e., positive, or negative) across all modalities and all

11 tasks at the same time point. The binary conjunction was performed at each time point spanning from -15 to 15 seconds relative to the block/event onset. For display purposes (Figure 1C), the mean percent change time course for each ROI was calculated by first averaging across subjects within each task, and these time courses were then averaged across all 11 tasks.

Results

Previous studies have mainly focused on the role of cortical networks in top-down and bottom-up dynamic modulation of attention[9, 67-69]. Meanwhile, subcortical arousal structures are mainly known for their role in controlling long-lasting states such as sleep-wake cycles[1], but their role in dynamic modulation of attention has been increasingly studied recently[5-7]. In the current study, we aim to investigate a shared transient pulse of activity in subcortical arousal systems that occurs with modulation of attention across 11 different tasks spanning four sensory modalities, including, vision, audition, taste, and touch with large sample sizes to ensure robustness of the results and that the observed networks are independent of the task design, type, or demands. This approach allows better isolation of brain activity due to dynamic transitions in attention from the activity due to particular stimuli/tasks. We performed a model-free fMRI analysis by calculating percent change in BOLD fMRI signals with respect to the mean of each fMRI run. To identify the statistically significant changes in percent change BOLD brain maps and time courses with respect to the baseline just prior to transitions in attention, we employed cluster-based permutation testing ($p < 0.05$). Binary and graded conjunctions were performed on the statistical brain maps and time courses to identify the shared subcortical and cortical regions across sensory modalities. Disjunction analyses were applied to the statistical brain maps to identify unique cortical and subcortical regions for each sensory modality.

Binary conjunction analysis showed a shared transient pulse of subcortical fMRI increases across all sensory modalities and tasks in the midbrain and central thalamus within four seconds from the stimulus onset (Fig. 1.A, 1.B). These increases were centered mainly on the midbrain reticular formation (MRF) and thalamic intralaminar central lateral nucleus (CL) which are key subcortical structures for arousal and attention modulation[1, 6, 23, 25, 57]. Shared fMRI increases across modalities extended into adjacent anatomical regions of the midbrain tegmentum and into other nearby thalamic nuclei such as the mediodorsal nucleus and ventrolateral nucleus bordering thalamic CL (See Supplementary Presentation S1 for binary conjunction maps in additional brain slices and time points). To investigate the timing of these changes, we performed a conjunction analysis of the mean time course of percent change fMRI signals in the MRF and thalamic CL nucleus across all tasks (Fig 1.C). This demonstrated a shared significant transient increase in both regions across all sensory modalities and tasks within four seconds from the stimulus onset, which remained significant for an additional 2-4 seconds before returning towards baseline. Thus, a transient pulse of fMRI activation was seen most consistently in the midbrain reticular formation and central thalamus during transitions of attention in a large data set across perceptual modalities and tasks.

Our binary conjunction approach employed stringent inclusion criteria where a region could be included in the conjunction only if it showed significance across all sensory modalities at the same time point. To pinpoint regions statistically significant across some sensory modalities, but not necessarily all of them, we conducted graded conjunction analyses. The graded conjunction analysis revealed subcortical increases and decreases less consistently shared across modalities,

not detectable through the strict binary conjunction that required the activity to be shared across all tasks. Through the graded conjunction analysis, we found early fMRI changes after stimulus onset overlapping several subcortical structures, including those in the pons, midbrain, hypothalamus, basal forebrain, amygdala, thalamus and basal ganglia (Fig. 2 and Table 2; see also Supplementary Presentation S1 for graded conjunction maps in additional brain slices and time points). In the pons, shared increases were noted in at least two sensory modalities 4 s after stimulus onset in the locus coeruleus, parabrachial nucleus, and pontine nucleus oralis. In the midbrain, in addition to the MRF, early shared increases were observed in the dorsal raphe, pedunculopontine tegmental nucleus, superior colliculi, and ventral tegmental area. In the thalamus, in addition to CL, consistent increases were seen in all modalities in adjacent central thalamic regions of the mediodorsal and ventrolateral nuclei. The nearby centromedian and ventral medial nuclei also showed increases in three or four modalities. Increases in at least two modalities were also seen in the lateral and posterior hypothalamus, as well as in the basal ganglia caudate, globus pallidus and subthalamic nucleus. Increases in only one modality were seen in the amygdala, nucleus basalis, nucleus accumbens and putamen. fMRI decreases were less consistently seen in subcortical structures at early times, with shared decreases seen across two sensory modalities in the amygdala, putamen and globus pallidus; and in one modality in the nucleus basalis.

To comprehensively delineate the brain networks outside subcortical regions that participate during transitions in attention across sensory modalities, we performed a whole-brain binary conjunction analysis to identify the involved cortical networks. The whole-brain conjunction showed transient cortical increases at early times in detection, arousal and salience networks,

including bilateral visual cortex, bilateral anterior insula and bilateral anterior cingulate/supplementary motor area (Fig. 3A). Early increases were also observed in attention and executive control networks, including the right anterior inferior parietal lobule, right superior parietal lobule, bilateral medial parietal cortex, and bilateral middle frontal gyrus (Fig. 3A). For cortical regions, we also conducted a graded conjunction analysis to identify fMRI changes present in some but not all sensory modalities. The graded conjunction analysis enabled identification of additional bilateral cortical regions showing less consistent increases across modalities at early times including the opercular part of the inferior frontal gyrus (Fig. 3B). In addition, although no early shared cortical fMRI decreases were observed across all sensory modalities, the graded conjunction analysis revealed early decreases in at least three modalities in default mode network areas, including the ventral medial prefrontal cortex, posterior cingulate/precuneus, and posterior inferior parietal lobule (Fig. 3C; see also Supplementary Presentation S1 for binary and graded conjunction maps of shared cortical changes in additional brain slices and time points).

To further validate our approach investigating shared changes across sensory modalities, we also analyzed changes specific to each modality. As already described for the binary and graded conjunctions analyses, we began by constructing binary conjunction maps across tasks within each modality to obtain changes for the four modalities (see Supplementary Presentation S2). We then used exclusive disjunction analyses to identify changes unique for each sensory modality. This approach retained only voxels that showed statistically significant increases or decreases for one modality but no others at each location in the brain. We found expected sensory modality-specific changes at early times after stimulus onset in both subcortical and cortical regions. Thus,

the subcortical disjunction analysis revealed fMRI increases in the lateral geniculate nucleus and pulvinar exclusively for visual tasks (Fig. 4A, B); increases in the superior olivary complex, medial geniculate nucleus, and inferior colliculus as well as decreases in the putamen exclusively for auditory tasks (Fig. 4D - F); increases in the nucleus solitarius, ventral posterior medial nucleus, amygdala and regions of the basal ganglia exclusively for the taste tasks (Fig. 4 G – I); and increases in the caudate nucleus as well as decreases in a portion of the putamen for tactile tasks (Fig. 4C). Cortical disjunction analyses likewise showed mainly expected changes unique to each sensory modality at early times after stimulus onset. These included increases in the fusiform gyrus and intraparietal sulcus for visual tasks (Figure 5A, B); increases in primary auditory cortex for auditory tasks (Fig. 5C, D); increases in the anterior insula and other regions for taste tasks (Fig. 5 E, F); and increases in primary somatosensory cortex along with changes in several other cortical regions for the tactile tasks (Fig. 5G, H; see also Supplementary Presentation S3 for disjunction maps for each sensory modality in additional brain slices and time points).

Discussion

We identified a shared subcortical arousal network across four sensory modalities – vision, audition, taste, and touch. The regions belonging to this network showed an early transient pulse of fMRI increases across 11 tasks within four seconds from the onset of task blocks and individual events. These increases were centered mainly on the MRF and thalamic intralaminar CL, structures pivotal for arousal and attention modulation. The time courses of percent change BOLD signals in the MRF and CL demonstrated a shared significant transient increase within four seconds from the stimulus onset. Besides CL, other nearby central thalamic nuclei

overlapped with the observed increases, including, mediodorsal, ventrolateral, centromedian, and ventral medial nuclei. In addition to the identified subcortical network, a shared cortical network was activated at the same time frame in regions important for signal detection, attentional salience and top-down control such as the visual cortex, anterior insula, anterior cingulate/supplementary motor area, anterior inferior parietal lobule, superior parietal lobule, medial parietal cortex, and middle frontal gyrus. At the same time frame (four seconds from stimulus onset), less consistent increases and decreases were observed in multiple arousal and/or attention-related subcortical areas in the pons, midbrain, hypothalamus, basal forebrain, basal ganglia, and amygdala. Cortically, less consistent increases were observed in several regions such as the opercular part of the inferior frontal gyrus associated with attention control, and decreases were observed in the default mode network. Collectively, these observations provide new insights into brain mechanisms of arousal and attention irrespective of sensory modality, presented stimuli, or task demands and could lead to improved targeted therapies for disorders of arousal, attention and consciousness.

Several models of attention suggested a potential role of subcortical networks in attention modulation[70-73], however, previous studies have mainly focused on the role of cortical large-scale networks in top-down and bottom-up attention regulation[9, 67-69]. Meanwhile, subcortical arousal networks have been mainly investigated for their involvement in controlling sustained changes of attention such as sleep-wake cycles[1, 57, 74]. Recently, the role of these subcortical networks in dynamic modulation of attention has been increasingly recognized. Previous studies suggested that arousal systems in the thalamus, upper brainstem and basal forebrain may contribute to dynamic modulation of attention and conscious perception[5, 6, 23-25]. This is further supported by

lesion studies in the brainstem and thalamus identifying a key role of these regions in conscious perception and attention control [75, 76]. Although findings of several recent studies highlighted the involvement of some subcortical structures in dynamic attention control[7, 77], the potential role of subcortical networks in modulating attention across sensory modalities has not been investigated.

An early bilateral pulse of increases was observed within the midbrain and central thalamus within four seconds from the stimulus onset. Notably, this observation is very early given the relatively low temporal resolution of fMRI, but represents the earliest time at which the rising phase of these increases reach statistical significance, whereas the peak occurs 1-2 seconds later. The midbrain and central thalamic increases were common across the four sensory modalities, including vision, audition, taste, and touch. This may reflect the common role of these regions in attention modulation irrespective of the sensory modality or the specific tasks/stimuli presented to the participants. Previous studies on healthy participants and patients with impaired consciousness suggested that the MRF and central thalamus are key subcortical structures in the modulation of attention[2-4, 13, 14, 16, 17]. Additionally, deep brain stimulation studies in human and animal models showed that stimulation of the central thalamus significantly improves arousal and restores consciouness[18, 19, 21, 22, 78, 79]. The early bilateral pulse of increases we identified within the MRF and central thalamus aligns with the findings from previous intracranial EEG and fMRI studies that investigated the role of these regions in conscious perception and dynamic modulation of attention across visual tasks requiring varying degrees of attention[6, 7]. Furthermore, our findings are consistent with a seminal positron emission tomography study that reported early cerebral blood flow increases in MRF and intralaminar thalamus while participants performed an attention-demanding reaction-time task [80].

Several neurotransmitters play an important role in attention and/or arousal modulation, including acetylcholine, glutamate, dopamine, noradrenaline, histamine, and orexin [81-83 84]. The current study identified various subcortical regions associated with attention modulation, each predominantly utilizing one or more of these neurotransmitters. Among the identified regions, pontine nucleus oralis, midbrain reticular formation, and central thalamus, primarily employ glutamate for attention control[2, 83, 85-88]. Other subcortical structures that we visualized with some involvement at early times, such as the parabrachial complex, pedunculopontine tegmental nucleus, and nucleus basalis utilize primarily acetylcholine, along with glutamate and GABA[83, 85, 89]. Meanwhile, the locus coeruleus, ventral tegmental area, and dorsal raphe use primarily noradrenaline[90, 91], dopamine[92], and serotonin[89, 93], respectively, although each contain other neurotransmitters as well. Furthermore, the posterior hypothalamus including the tuberomammillary nucleus and the lateral hypothalamus are recognized for their roles in releasing histamine and orexin, respectively, to modulate arousal [74, 84, 94, 95]. Additional subcortical structures showed significant changes with respect to baseline across some sensory modalities including the superior colliculi, caudate, putamen, globus pallidus, nucleus accumbens, and amygdala. Previous studies indicated that the amygdala plays key roles in attention, arousal, and decision making[96]. The superior colliculus is mainly known for its role in stimulus detection and modulation of spatial attention[97-101]. Basal ganglia structures including the caudate, putamen, globus pallidus, and nucleus accumbens were found to control sleep-wake transitions [102] and play a role in recovery of consciousness after a brain injury[103, 104]. Although we identified BOLD decreases in basal ganglia for some modalities, these decreases do not necessarily reflect decreases in neural activity[105, 106].

We identified a shared cortical network that includes regions involved in event detection, bottom-up attentional salience, top-down attentional control, conscious perception, and motor preparation[6-11, 107, 108]. The identified regions included anterior insula and anterior cingulate/supplementary motor area which are key structures in the salience network as well as additional regions belonging to the attention and executive control networks, including regions of the parietal lobe and lateral frontal cortex[6-11]. Interestingly, consistent early cortical increases across modalities also included the primary visual cortex, which may speak to the potential cross-modal function of some primary cortical regions in sensory processing[109]. Less consistent increases were observed in the opercular part of the inferior frontal gyrus, known to play a role in attention control[110-112], and less consistent decreases were observed in well-known default mode areas, including ventromedial frontal cortex, precuneus, and the posterior inferior parietal lobule[6, 7, 113-116].

Our findings support a data-driven hypothesis we introduced previously to describe the sequence of neural mechanisms required to produce conscious perceptual awareness of external sensory stimuli[26]. In particular, the transient pulse of activation in subcortical arousal systems observed across sensory modalities in the current study fits in this framework. We hypothesize that for a sensory stimulus to be consciously perceived, it has to be first detected by the primary cortex and other cortical and subcortical signal detection circuits. Next, a dynamic transient pulse of activity in subcortical and cortical arousal systems modulates attention and facilitates subsequent widespread signal processing necessary for conscious perception. Then, potentially competing activity in the default mode network is switched off. Finally, a broad wave of hierarchical

processing progresses through association cortical areas to fully process the event before it is encoded in memory systems. Our present findings strengthen this hypothesis[26] by identifying a highly consistent transient pulse of increased fMRI activity in midbrain and central thalamus shared across visual, tactile, auditory and taste stimuli, associated with transitions of attention in tasks requiring sensory perception.

The disjunction analysis helped to validate our approach by showing cortical and subcortical regions that are well-known to be associated with each sensory modality. For instance, visual tasks showed unique activations in lateral geniculate nucleus, pulvinar, fusiform gyrus and the intraparietal sulcus[117, 118], while auditory tasks showed unique activations in superior olivary nuclear complex, inferior colliculus, medial geniculate nucleus, and primary auditory cortex[119]. Unique activations for taste included the nucleus solitarius, ventral posterior medial nucleus, amygdala, and anterior insular cortex[120, 121]. Additionally, unique increases were observed for touch in the caudate nucleus and primary somatosensory cortex[122, 123]. Unique decreases in different parts of the putamen were found in audition and touch. Previous studies have shown that the putamen is involved in attentive processing of auditory or tactile stimuli, but with increased BOLD activity[124-126]. Thus, the decreases observed in the current study need to be further investigated[106].

Our study has several limitations that should be addressed in future work. Techniques have been proposed to improve inter-subject subcortical co-registration, but are so far not widely used [127, 128]. These approaches typically require high computational costs, rendering their application impractical in our present study due to the substantial sample size, which exceeded 1,500

participants. Because we did not use such approaches in the current study, we were cautious to avoid making strong conclusions on the voxel level, particularly if the activations/deactivations were not centered on anatomically known structures. Although we included large sample sizes to identify the shared subcortical and cortical networks, the analyzed datasets were not balanced across sensory modalities due to the limited availability of tasks from certain sensory modalities such as taste and touch. No olfaction tasks suiting our analysis purposes were available. Future studies should aim to balance the sample sizes across sensory modalities, and should include more taste and tactile tasks if available. Inclusion of olfaction tasks is an important future direction, particularly because some olfactory signaling pathways bypass the thalamus. This will help to further identify the shared changes across all senses. Although fMRI provides comprehensive anatomical mapping of cortical and subcortical structures not available with more spatially limited human electrophysiological methods, it has lower temporal resolution, and therefore may provide limited information about the sequence of activations/deactivations within the observed networks. Further investigation of these networks could be performed in animal models through direct electrophysiological recordings, or in human studies with availability of subcortical depth electrodes to identify the temporal dynamics of these networks. In addition, regions that are common to some but not all sensory modalities need to be investigated further to identify why they are specific to certain sensory modalities but not others.

In summary, although previous work in conscious perception and attention modulation has recognized the regions we found, prior studies were conducted predominantly in individual sensory modalities. Our approach of analyzing different tasks spanning multiple sensory modalities and with overall large sample size, enabled us to identify changes independent of the

task design, demands or stimulus type. We found the most consistent subcortical change associated with transitions in attention was a transient increase in activity in the MRF and central thalamus. These subcortical changes were accompanied by consistent increases in activity in cortical detection, arousal and salience networks, as well as by less consistent changes in multiple other subcortical and cortical regions. Further investigation of the shared subcortical arousal systems participating across sensory modalities could lead to improved targeted therapies for disorders of arousal, attention and consciousness[78, 129-131] and a better understanding of the complex spatiotemporal mechanisms of normal brain function.

Acknowledgements

This work was supported by the NIH R01 NS134655 (to H.B.), the Mark Loughridge and Michele Williams Foundation, and the Betsy and Jonathan Blattmachr family. A.H. was supported by the German Research Foundation (Deutsche Forschungsgemeinschaft, 424778381 – TRR 295), Deutsches Zentrum für Luft- und Raumfahrt (DynaSti grant within the EU Joint Programme Neurodegenerative Disease Research, JPND), the National Institutes of Health (R01MH130666, 1R01NS127892-01, 2R01 MH113929 & UM1NS132358) as well as the New Venture Fund (FFOR Seed Grant). A.H. reports lecture fees for Boston Scientific and is a consultant for FxNeuromodulation and Abbott."

Data Availability

Datasets included in the study are publicly available through OpenNeuro and Human Connectome Project websites.

Code Availability

Analysis codes for this study will be publicly available upon publication here:

https://github.com/BlumenfeldLab/Khalaf-et-al_2024

References

1. Steriade MM, McCarley RW. Brain Control of Wakefulness and Sleep. Springer; 2nd ed 2010.

2. Edlow BL, Takahashi E, Wu ON, et al. Neuroanatomic Connectivity of the Human Ascending Arousal System Critical to Consciousness and Its Disorders. J Neuropath Exp Neur 2012;71:531-546.

3. Schiff ND. Central thalamic contributions to arousal regulation and neurological disorders of consciousness. Ann N Y Acad Sci 2008;1129:105-118.

4. Schiff ND, Plum F. The role of arousal and "gating" systems in the neurology of impaired consciousness. J Clin Neurophysiol 2000;17:438-452.

5. Sarter M, Lustig C. Forebrain Cholinergic Signaling: Wired and Phasic, Not Tonic, and Causing Behavior. J Neurosci 2020;40:712-719.

6. Li R, Ryu JH, Vincent P, et al. The pulse: transient fMRI signal increases in subcortical arousal systems during transitions in attention. Neuroimage 2021;232:117873.

7. Kronemer SI, Aksen M, Ding JZ, et al. Human visual consciousness involves large scale cortical and subcortical networks independent of task report and eye movement activity. Nat Commun 2022;13:7342.

8. Barry RJ, Steiner GZ, De Blasio FM. Event-related EEG time-frequency analysis and the Orienting Reflex to auditory stimuli. Psychophysiology 2012;49:744-755.

9. Corbetta M, Shulman GL. Control of goal-directed and stimulus-driven attention in the brain. Nat Rev Neurosci 2002;3:201-215.

10. Menon V, Uddin LQ. Saliency, switching, attention and control: a network model of insula function. Brain Struct Funct 2010;214:655-667.

11. Seeley WW, Menon V, Schatzberg AF, et al. Dissociable intrinsic connectivity networks for salience processing and executive control. J Neurosci 2007;27:2349-2356.

12. Janacsek K, Evans TM, Kiss M, Shah L, Blumenfeld H, Ullman MT. Subcortical Cognition: The Fruit Below the Rind. Annu Rev Neurosci 2022;45:361-386.

13. Li R, Hu C, Wang L, et al. Disruption of functional connectivity among subcortical arousal system and cortical networks in temporal lobe epilepsy. Brain imaging and behavior 2019:1-10.

14. Nagai Y, Critchley HD, Featherstone E, Fenwick PB, Trimble MR, Dolan RJ. Brain activity relating to the contingent negative variation: an fMRI investigation. Neuroimage 2004;21:1232-1241.

15. Setzer B, Fultz NE, Gomez DEP, et al. A temporal sequence of thalamic activity unfolds at transitions in behavioral arousal state. Nature Communications 2022;13.

16. Van der Werf YD, Witter MP, Groenewegen HJ. The intralaminar and midline nuclei of the thalamus. Anatomical and functional evidence for participation in processes of arousal and awareness. Brain research Brain research reviews 2002;39:107-140.

17. Yanaka HT, Saito DN, Uchiyama Y, Sadato N. Neural substrates of phasic alertness: a functional magnetic resonance imaging study. Neurosci Res 2010;68:51-58.

18. Arnts H, Tewarie P, van Erp W, et al. Deep brain stimulation of the central thalamus restores arousal and motivation in a zolpidem-responsive patient with akinetic mutism after severe brain injury. Sci Rep 2024;14:2950.

19. Redinbaugh MJ, Phillips JM, Kambi NA, et al. Thalamus Modulates Consciousness via Layer-Specific Control of Cortex. Neuron 2020;106:66-75 e12.

20. Schiff ND, Giacino JT, Kalmar K, et al. Behavioural improvements with thalamic stimulation after severe traumatic brain injury. Nature 2007;448:600-U610.

21. Tasserie J, Uhrig L, Sitt JD, et al. Deep brain stimulation of the thalamus restores signatures of consciousness in a nonhuman primate model. Sci Adv 2022;8:eabl5547.

22. Xu J, Galardi MM, Pok B, et al. Thalamic Stimulation Improves Postictal Cortical Arousal and Behavior. J Neurosci 2020;40:7343-7354.

23. Schiff ND, Shah SA, Hudson AE, Nauvel T, Kalik SF, Purpura KP. Gating of attentional effort through the central thalamus. J Neurophysiol 2013;109:1152-1163.

24. Raver SM, Lin SC. Basal forebrain motivational salience signal enhances cortical processing and decision speed. Front Behav Neurosci 2015;9:277.

25. Kinomura S, Larsson J, Gulyas B, Roland PE. Activation by attention of the human reticular formation and thalamic intralaminar nuclei. Science 1996;271:512-515.

26. Blumenfeld H. Brain Mechanisms of Conscious Awareness: Detect, Pulse, Switch, and Wave. Neuroscientist 2023;29:9-18.

27. Koch C, Massimini M, Boly M, Tononi G. Neural correlates of consciousness: progress and problems (vol 17, pg 307, 2016). Nat Rev Neurosci 2016;17:395-395.

28. Buckner RL, Bandettini PA, O'Craven KM, et al. Detection of cortical activation during averaged single trials of a cognitive task using functional magnetic resonance imaging. Proc Natl Acad Sci U S A 1996;93:14878-14883.

29. Visscher KM, Miezin FM, Kelly JE, et al. Mixed blocked/event-related designs separate transient and sustained activity in fMRI. Neuroimage 2003;19:1694-1708.

30. Dosenbach NU, Fair DA, Miezin FM, et al. Distinct brain networks for adaptive and stable task control in humans. Proceedings of the National Academy of Sciences of the United States of America 2007;104:11073-11078.

31. Fox MD, Snyder AZ, Vincent JL, Corbetta M, Van Essen DC, Raichle ME. The human brain is intrinsically organized into dynamic, anticorrelated functional networks. Proceedings of the National Academy of Sciences of the United States of America 2005;102:9673-9678.

32. Shulman GL, Fiez JA, Corbetta M, et al. Common Blood Flow Changes across Visual Tasks: II. Decreases in Cerebral Cortex. J Cogn Neurosci 1997;9(5):648-663.

33. Fox MD, Snyder AZ, Barch DM, Gusnard DA, Raichle ME. Transient BOLD responses at block transitions. Neuroimage 2005;28:956-966.

34. Paret C, Kluetsch R, Ruf M, et al. Transient and sustained BOLD signal time courses affect the detection of emotion-related brain activation in fMRI. Neuroimage 2014;103:522-532.

35. Uludag K. Transient and sustained BOLD responses to sustained visual stimulation. Magn Reson Imaging 2008;26:863-869.

36. Gonzalez-Castillo J, Saad ZS, Handwerker DA, Inati SJ, Brenowitz N, Bandettini PA. Whole-brain, time-locked activation with simple tasks revealed using massive averaging and model-free analysis. Proceedings of the National Academy of Sciences of the United States of America 2012;109:5487-5492.

37. Guo JN, Kim R, Chen Y, et al. Impaired consciousness in patients with absence seizures investigated by functional MRI, EEG, and behavioural measures: a cross-sectional study. Lancet Neurol 2016;15:1336-1345.

38. Barch DM, Burgess GC, Harms MP, et al. Function in the human connectome: task-fMRI and individual differences in behavior. Neuroimage 2013;80:169-189.

39. Van Essen DC, Smith SM, Barch DM, Behrens TE, Yacoub E, Ugurbil K. The WU-Minn Human Connectome Project: an overview. Neuroimage 2013;80:62-79.

40. Poldrack RA, Congdon E, Triplett W, et al. A phenome-wide examination of neural and cognitive function. Sci Data 2016;3.

41. Pernet CR, McAleer P, Latinus M, et al. The human voice areas: Spatial organization and inter-individual variability in temporal and extra-temporal cortices. Neuroimage 2015;119:164-174.

42. Czarnecka M, Raczy K, Szewczyk J, et al. Overlapping but separate number representations in the intraparietal sulcus-Probing format- and modality-independence in sighted Braille readers. Cortex 2023;162:65-80.

43. Dalenberg JR, Patel BP, Denis R, et al. Short-Term Consumption of Sucralose with, but Not without, Carbohydrate Impairs Neural and Metabolic Sensitivity to Sugar in Humans. Cell Metab 2020;31:493-+.

44. Veldhuizen MG, Farruggia MC, Gao X, Nakamura Y, Green BG, Small DM. Identification of an Amygdala Thalamic Circuit That Acts as a Central Gain Mechanism in Taste Perceptions. Journal of Neuroscience 2020;40:5051-5062.

45. WU-Minn. HCP 1200 subjects data release reference manual. 2017. Accessed at: https://www.humanconnectome.org

46. Delgado MR, Nystrom LE, Fissell C, Noll DC, Fiez JA. Tracking the hemodynamic responses to reward and punishment in the striatum. J Neurophysiol 2000;84:3072-3077.

47. Smith R, Keramatian K, Christoff K. Localizing the rostrolateral prefrontal cortex at the individual level. Neuroimage 2007;36:1387-1396.

48. Caceres A, Hall DL, Zelaya FO, Williams SCR, Mehta MA. Measuring fMRI reliability with the intra-class correlation coefficient. Neuroimage 2009;45:758-768.

49. Drobyshevsky A, Baumann SB, Schneider W. A rapid fMRI task battery for mapping of visual, motor, cognitive, and emotional function. Neuroimage 2006;31:732-744.

50. Castelli F, Happé F, Frith U, Frith C. Movement and mind:: A functional imaging study of perception and interpretation of complex intentional movement patterns. Neuroimage 2000;12:314-325.

51. Buckner RL, Krienen FM, Castellanos A, Diaz JC, Yeo BTT. The organization of the human cerebellum estimated by intrinsic functional connectivity. Journal of Neurophysiology 2011;106:2322-2345.

52. Binder JR, Gross WL, Allendorfer JB, et al. Mapping anterior temporal lobe language areas with fMRI: A multicenter normative study. Neuroimage 2011;54:1465-1475.

53. Glasser MF, Sotiropoulos SN, Wilson JA, et al. The minimal preprocessing pipelines for the Human Connectome Project. Neuroimage 2013;80:105-124.

54. Power J, KA B, AZ S, BL S, SE P. Spurious but systematic correlations in functional connectivity MRI networks arise from subject motion. Neuroimage 2012;59:2142-2154.

55. Smyser C, Inder T, Shimony J, et al. Longitudinal Analysis of Neural Network Development in Preterm Infants. Cerebral Cortex 2010;20:2852-2862.

56. Bai X, Vestal M, Berman R, et al. Dynamic time course of typical childhood absence seizures: EEG, behavior, and functional magnetic resonance imaging. J Neurosci 2010;30:5884-5893.

57. Edlow BL, Olchanyi M, Freeman HJ, et al. Multimodal MRI reveals brainstem connections that sustain wakefulness in human consciousness. Sci Transl Med 2024;16:eadj4303.

58. Niemann K, Mennicken VR, Jeanmonod D, Morel A. The morel stereotactic atlas of the human thalamus: Atlas-to-MR registration of internally consistent Canonical Model. Neuroimage 2000;12:601-616.

59. Prodoehl J, Yu H, Little DM, Abraham I, Vaillancourt DE. Region of interest template for the human basal ganglia: Comparing EPI and standardized space approaches. Neuroimage 2008;39:956-965.

60. Neudorfer C, Germann J, Elias GJB, Gramer R, Boutet A, Lozano AM. A high-resolution magnetic resonance imaging atlas of the human hypothalamic region. Sci Data 2020;7.

61. Xiao Y, Fonov V, Chakravarty MM, et al. A dataset of multi-contrast population-averaged brain MRI atlases of a Parkinson′s disease cohort. Data Brief 2017;12:370-379.

62. Maris E, Oostenveld R. Nonparametric statistical testing of EEG- and MEG-data. J Neurosci Methods 2007;164:177-190.

63. Handwerker D, Ollinger J, D'Esposito M. Variation of BOLD hemodynamic responses across subjects and brain regions and their effects on statistical analyses. Neuroimage 2004;21:1639-1651.

64. Bansal R, Peterson BS. Cluster-level statistical inference in fMRI datasets: The unexpected behavior of random fields in high dimensions. Magn Reson Imaging 2018;49:101-115.

65. Groppe DM, Urbach TP, Kutas M. Mass univariate analysis of event-related brain potentials/fields I: a critical tutorial review. Psychophysiology 2011;48:1711-1725.

66. Edlow BL, Mareyam A, Horn A, et al. Tesla MRI of the human brain at 100 micron resolution. Sci Data 2019;6.

67. Dosenbach NU, Fair DA, Cohen AL, Schlaggar BL, Petersen SE. A dual-networks architecture of top-down control. Trends in Cognitive Sciences 2008;12:99-105.

68. Fortenbaugh FC, DeGutis J, Esterman M. Recent theoretical, neural, and clinical advances in sustained attention research. Ann N Y Acad Sci 2017;1396:70-91.

69. Helfrich RF, Breska A, Knight RT. Neural entrainment and network resonance in support of top-down guided attention. Curr Opin Psychol 2019;29:82-89.

70. Mesulam MM. A cortical network for directed attention and unilateral neglect. Ann Neurol 1981;10:309-325.

71. Mohanty A, Gitelman DR, Small DM, Mesulam MM. The spatial attention network interacts with limbic and monoaminergic systems to modulate motivation-induced attention shifts. Cereb Cortex 2008;18:2604-2613.

72. Posner MI, Rothbart MK. Research on attention networks as a model for the integration of psychological science. Annu Rev Psychol 2007;58:1-23.

73. Posner MI, Sheese BE, Odludas Y, Tang Y. Analyzing and shaping human attentional networks. Neural Netw 2006;19:1422-1429.

74. Saper CB, Fuller PM, Pedersen NP, Lu J, Scammell TE. Sleep State Switching. Neuron 2010;68:1023-1042.

75. Parvizi J, Damasio AR. Neuroanatomical correlates of brainstem coma. Brain 2003;126:1524-1536.

76. Bogen JE. On the neurophysiology of consciousness: I. An overview. Conscious Cogn 1995;4:52-62.

77. Levinson M, Podvalny E, Baete SH, He BJ. Cortical and subcortical signatures of conscious object recognition. Nat Commun 2021;12:2930.

78. Schiff ND, Giacino JT, Kalmar K, et al. Behavioural improvements with thalamic stimulation after severe traumatic brain injury. Nature 2007;448:600-603.

79. Martin RA, Cukiert A, Blumenfeld H. Short-term changes in cortical physiological arousal measured by electroencephalography during thalamic centromedian deep brain stimulation. Epilepsia 2021;62:2604-2614.

80. Kinomura S, Larsson J, Gulyas B, Roland PE. Activation by attention of the human reticular formation and thalamic intralaminar nuclei. Science 1996;271:512.

81. Burk JA, Blumenthal SA, Maness EB. Neuropharmacology of attention. Eur J Pharmacol 2018;835:162-168.

82. Thiele A, Bellgrove MA. Neuromodulation of Attention. Neuron 2018;97:769-785.

83. Motelow J, Blumenfeld H. Consciousness and Subcortical Arousal Systems. In: Faingold CL, Blumenfeld H (Eds), Neuronal Networks in Brain Function, CNS Disorders, and Therapeutics, Elsevier 2014; Ch 21, p. 277-298.

84. Mather M. How Arousal-Related Neurotransmitter Systems Compensate for Age-Related Decline. In: Thomas A, Gutchess A, eds. The Cambridge Handbook of Cognitive Aging: A Life Course Perspective: Cambridge University Press, 2020: 101 - 120.

85. Blumenfeld H. Neuroanatomical Basis of Consciousness. In: The Neurology of Consciousness, 2nd Edition Eds: O Gosseries, S Laureys, G Tononi Elsevier, Ltd 2015;Ch 1.

86. Jones BE. Arousal and sleep circuits. Neuropsychopharmacology 2020;45:6-20.

87. Parvizi J, Damasio A. Consciousness and the brainstem. Cognition 2001;79:135-159.

88. Shin A, Park S, Shin W, et al. A brainstem-to-mediodorsal thalamic pathway mediates sound-induced arousal from slow-wave sleep. Curr Biol 2023;33:875-+.

89. Blumenfeld H. Arousal and Consciousness in Focal Seizures. Epilepsy Curr 2021;21:353-359.

90. Mazancieux A, Mauconduit F, Amadon A, Willem de Gee J, Donner TH, Meyniel F. Brainstem fMRI signaling of surprise across different types of deviant stimuli. Cell Rep 2023;42:113405.

91. Ross JA, Van Bockstaele EJ. The Locus Coeruleus- Norepinephrine System in Stress and Arousal: Unraveling Historical, Current, and Future Perspectives. Front Psychiatry 2021;11.

92. Morales M, Margolis EB. Ventral tegmental area: cellular heterogeneity, connectivity and behaviour. Nat Rev Neurosci 2017;18:73-85.

93. Li A, Li R, Ouyang PR, et al. Dorsal raphe serotonergic neurons promote arousal from isoflurane anesthesia. Cns Neurosci Ther 2021;27:941-950.

94. Anaclet C, Parmentier R, Ouk K, et al. Orexin/Hypocretin and Histamine: Distinct Roles in the Control of Wakefulness Demonstrated Using Knock-Out Mouse Models. Journal of Neuroscience 2009;29:14423-14438.

95. Saper CB. Staying awake for dinner: hypothalamic integration of sleep, feeding, and circadian rhythms. Prog Brain Res 2006;153:243-252.

96. Pessoa L. Emotion and cognition and the amygdala: From "what is it?" to "what's to be done?" (Reprinted from Neuropsychologia, vol 48, pg 3416-3429, 2010). Neuropsychologia 2011;49:681-694.

97. Asadollahi A, Knudsen EI. Spatially precise visual gain control mediated by a cholinergic circuit in the midbrain attention network. Nat Commun 2016;7:13472.

98. Bollimunta A, Bogadhi AR, Krauzlis RJ. Comparing frontal eye field and superior colliculus contributions to covert spatial attention. Nat Commun 2018;9:3553.

99. Knudsen EI. Control from below: the role of a midbrain network in spatial attention. Eur J Neurosci 2011;33:1961-1972.

100. Mysore SP, Knudsen EI. A shared inhibitory circuit for both exogenous and endogenous control of stimulus selection. Nat Neurosci 2013;16:473-478.

101. Wang L, Herman JP, Krauzlis RJ. Neuronal modulation in the mouse superior colliculus during covert visual selective attention. Sci Rep 2022;12:2482.

102. Lazarus M, Chen JF, Urade Y, Huang ZL. Role of the basal ganglia in the control of sleep and wakefulness. Curr Opin Neurobiol 2013;23:780-785.

103. Edlow BL, Claassen J, Schiff ND, Greer DM. Recovery from disorders of consciousness: mechanisms, prognosis and emerging therapies. Nat Rev Neurol 2021;17:135-156.

104. Schiff ND. Recovery of consciousness after brain injury: a mesocircuit hypothesis. Trends Neurosci 2010;33:1-9.

105. Cerri DH, Albaugh DL, Walton LR, et al. Distinct neurochemical influences on fMRI response polarity in the striatum. Nat Commun 2024;15:1916.

106. Mishra AM, Ellens DJ, Schridde U, et al. Where fMRI and electrophysiology agree to disagree: corticothalamic and striatal activity patterns in the WAG/Rij rat. J Neurosci 2011;31:15053-15064.

107. Barcelo F. The Madrid card sorting test (MCST): a task switching paradigm to study executive attention with event-related potentials. Brain research Brain research protocols 2003;11:27-37.

108. Kincade JM, Abrams RA, Astafiev SV, Shulman GL, Corbetta M. An event-related functional magnetic resonance imaging study of voluntary and stimulus-driven orienting of attention. J Neurosci 2005;25:4593-4604.

109. Teichert M, Bolz J. How Senses Work Together: Cross-Modal Interactions between Primary Sensory Cortices. Neural Plast 2018;2018:5380921.

110. Cazzoli D, Kaufmann BC, Paladini RE, Muri RM, Nef T, Nyffeler T. Anterior insula and inferior frontal gyrus: where ventral and dorsal visual attention systems meet. Brain Commun 2021;3:fcaa220.

111. Chong TT, Williams MA, Cunnington R, Mattingley JB. Selective attention modulates inferior frontal gyrus activity during action observation. Neuroimage 2008;40:298-307.

112. Hampshire A, Chamberlain SR, Monti MM, Duncan J, Owen AM. The role of the right inferior frontal gyrus: inhibition and attentional control. Neuroimage 2010;50:1313-1319.

113. Herman WX, Smith RE, Kronemer SI, et al. A Switch and Wave of Neuronal Activity in the Cerebral Cortex During the First Second of Conscious Perception. Cereb Cortex 2019;29:461-474.

114. Li J, Kronemer SI, Herman WX, et al. Default mode and visual network activity in an attention task: Direct measurement with intracranial EEG. Neuroimage 2019;201:116003.

115. Raichle ME, Snyder AZ. A default mode of brain function: a brief history of an evolving idea. Neuroimage 2007;37:1083-1090.

116. Singh K, Fawcett I. Transient and linearly graded deactivation of the human default-mode network by a visual detection task. Neuroimage 2008;41:100-112.

117. Gupta M, Ireland AC, Bordoni B. Neuroanatomy, Visual Pathway. StatPearls. Treasure Island (FL) ineligible companies. Disclosure: Ashley Ireland declares no relevant financial relationships with ineligible companies. Disclosure: Bruno Bordoni declares no relevant financial relationships with ineligible companies.2024.

118. Singh-Curry V, Husain M. The functional role of the inferior parietal lobe in the dorsal and ventral stream dichotomy. Neuropsychologia 2009;47:1434-1448.

119. Peterson DC, Reddy V, Launico MV, Hamel RN. Neuroanatomy, Auditory Pathway. StatPearls. Treasure Island (FL) ineligible companies. Disclosure: Vamsi Reddy declares no relevant financial relationships with ineligible companies. Disclosure: Marjorie Launico declares no relevant financial relationships with ineligible companies. Disclosure: Renee Hamel declares no relevant financial relationships with ineligible companies.2024.

120. Avery JA, Liu AG, Ingeholm JE, Riddell CD, Gotts SJ, Martin A. Taste Quality Representation in the Human Brain. J Neurosci 2020;40:1042-1052.

121. Kawakami S, Sato H, Sasaki AT, et al. The Brain Mechanisms Underlying the Perception of Pungent Taste of Capsaicin and the Subsequent Autonomic Responses. Front Hum Neurosci 2015;9:720.

122. Kitada R, Doizaki R, Kwon J, et al. Brain networks underlying tactile softness perception: A functional magnetic resonance imaging study. Neuroimage 2019;197:156-166.

123. Yeon J, Kim J, Ryu J, Park JY, Chung SC, Kim SP. Human Brain Activity Related to the Tactile Perception of Stickiness. Front Hum Neurosci 2017;11:8.

124. Opitz B, Schroger E, von Cramon DY. Sensory and cognitive mechanisms for preattentive change detection in auditory cortex. Eur J Neurosci 2005;21:531-535.

125. Peller M, Zeuner KE, Munchau A, et al. The basal ganglia are hyperactive during the discrimination of tactile stimuli in writer's cramp. Brain 2006;129:2697-2708.

126. Halder S, Leinfelder T, Schulz SM, Kubler A. Neural mechanisms of training an auditory event-related potential task in a brain-computer interface context. Human brain mapping 2019;40:2399-2412.

127. Balakrishnan G, Zhao A, Sabuncu MR, Guttag J, Dalca AV. VoxelMorph: A Learning Framework for Deformable Medical Image Registration. IEEE Trans Med Imaging 2019.

128. Cheng J, Dalca AV, Fischl B, Zollei L, Alzheimer's Disease Neuroimaging I. Cortical surface registration using unsupervised learning. Neuroimage 2020;221:117161.

129. Schiff ND, Giacino JT, Butson CR, et al. Thalamic deep brain stimulation in traumatic brain injury: a phase 1, randomized feasibility study. Nat Med 2023;29:3162-3174.

130. Kundishora AJ, Gummadavelli A, Ma C, et al. Restoring Conscious Arousal During Focal Limbic Seizures with Deep Brain Stimulation. Cereb Cortex 2017;27:1964-1975.

131. Gummadavelli A, Kundishora AJ, Willie JT, et al. Improving level of consciousness in epilepsy with neurostimulation. Neurosurgical Focus 2015;38(6):E10.

Figure Legends

Figure 1. Midbrain and central thalamus show shared subcortical early activations (increases), observed in 11 tasks across four sensory modalities, including, vision, audition, taste, and touch. These shared activations reached statistical significance within four seconds from block/event onset. Cluster-based permutation testing ($p < 0.05$) was employed to identify the statistically significant changes in percentage change BOLD brain maps and time courses with respect to the baseline before block/event onset for each sensory task. Binary conjunction analysis was then applied across all tasks to identify subcortical regions and time points sharing activations/deactivations across tasks and sensory modalities. (A) Axial, coronal, and sagittal MRI slices in the midbrain showing the spatial extent of the observed shared activations 4s after stimulus onset, mainly centered on the midbrain reticular formation (MRF). (B) Axial, coronal, and sagittal MRI slices showing the spatial extent of the observed activations in the thalamus 4s after stimulus onset, centered on the intralaminar central lateral (CL) nucleus. (A, B) for additional brain slices and time points see Supplementary Presentation S1. (C) Mean percent change BOLD time courses across the 11 tasks from two anatomical ROIs, MRF and CL, obtained from the Harvard Ascending Arousal Network atlas and the Morel atlas, respectively. The significant time points shared across tasks (permutation based statistics followed by conjunction analysis), marked on the top of the time courses, began 4 seconds after block/event onset in both the MRF and thalamic CL. Data are from 11 tasks obtained across a total of 1,561 participants.

Figure 2. Graded conjunction analysis revealed additional subcortical changes shared less consistently across sensory modalities. This method, which is less stringent than binary conjunction, highlights shared activations (increases) and deactivations (decreases) even if they do not occur across all sensory modalities. The activations and deactivations shown are from four seconds after block/event onset. Spatiotemporal cluster-based permutation testing ($p < 0.05$) was employed to identify the statistically significant changes in percentage change BOLD brain maps with respect to the baseline before block/event onset for each task, and binary conjunction revealed shared changes within each of the four sensory modalities. Graded conjunction analysis was then applied across the four sensory modalities to identify subcortical regions with shared activations/deactivations, and shared changes were graded from 0 to 4. (A – E) shared subcortical activations; (F) shared subcortical deactivations. For additional brain slices and time points of the graded conjunction analysis please see Supplementary Presentation S1. Locus ceruleus (LC), pontine nucleus oralis (PnO), pedunculopontine tegmental nucleus (PPN), ventral tegmental area (VTA), dorsal raphe (DR), amygdala (Amyg), mibrain reticular formation (MRF), lateral hypothalamus (LH), nucleus basalis (NB), nucleus accumbens (NA), posterior hypothalamus (PH), subthalamic nucleus (STN), superior collicululus (SC), caudate nucleus (Caud), thalamic central lateral nucleus (CL), thalamic centromedian nucleus (CM), thalamic ventrolateral nucleus (VL). Same data and participants as in Figure 1.

Figure 3. Shared cortical fMRI activations (increases) and deactivations (decreases) four seconds after block/event onset, obtained from whole brain analaysis. (A) Binary conjunction analysis required shared activity across the 11 tasks and four sensory modalities. Top row, axial slices; bottom row, surface views. (B) Graded conjunction analysis showing number of

modalities sharing cortical activations (significant fMRI increases) across the four sensory modalities. Top row, axial views; bottom rows surface views. (C) Graded conjunction analysis for deactivations across modalities. Top row, axial views; bottom rows surface views. For additional brain slices and time points of the binary and graded conjunction analyses please see Supplementary Presentation S1. Anterior insula (AI), anterior cingulate/supplementary motor area (AC/SMA), primary visual cortex (V1), anterior inferior parietal lobule (AIPL), superior parietal lobule (SPL), medial parietal cortex (MP), middle frontal gyrus (MFG), inferior frontal gyrus/frontal operculum (IF), ventral medial frontal cortex (VMFC), posterior cingulate (PC), and posterior inferior parietal lobule (PIPL). Same data and participants as in Figure 1.

Figure 4. Unique subcortical activations (increases) and deactivations (decreases) for each of the four sensory modalities (vision, audition, taste, and touch) observed four seconds after block/event onset. Exclusive disjunction analysis identified statistically significant subcortical changes present in each modality alone but in none of the other sensory modalities. (A, B) Visual disjunction analysis. (C) Tactile disjunction analysis. (D – F) Auditory disjunction analysis. (G – I) Taste disjunction analysis. For additional brain slices and time points of the disjunction analyses for each modality please see Supplementary Presentation S3. Lateral geniculate nucleus (LGN), pulvinar (Pulv), putamen (Put), caudate nucleus (Caud), superior olivary nuclear complex (SOC), medial geniculate nucleus (MGN), inferior colliculi (IC), nucleus solitarius (NS), amygdala (Amyg), globus pallidus (GP), ventral posterior medial nucleus (VPM). Same data and participants as in Figure 1.

Figure 5. Unique cortical activations (increases) and deactivations (decreases) for each of the four sensory modalities (vision, audition, taste, and touch) observed four seconds after block/event onset. Exclusive disjunction analysis identified statistically significant cortical changes present in each modality alone but in none of the other sensory modalities. (A, B) Visual disjunction analysis. (C, D) Auditory disjunction analysis. (E, F) Taste disjunction analysis. (G, H) Tactile disjunction analysis. (A, C, E, G) Axial brain slices. (B, D, F, H) Left hemisphere surface views. For additional brain slices and time points of the disjunction analyses for each modality please see Supplementary Presentation S3. Fusiform gyrus (FG), intraparietal sulcus (IPS), primary auditory cortex (Au1), anterior insula (AI), primary somatosensory cortex (S1). Same data and participants as in Figure 1.

Figure 1:

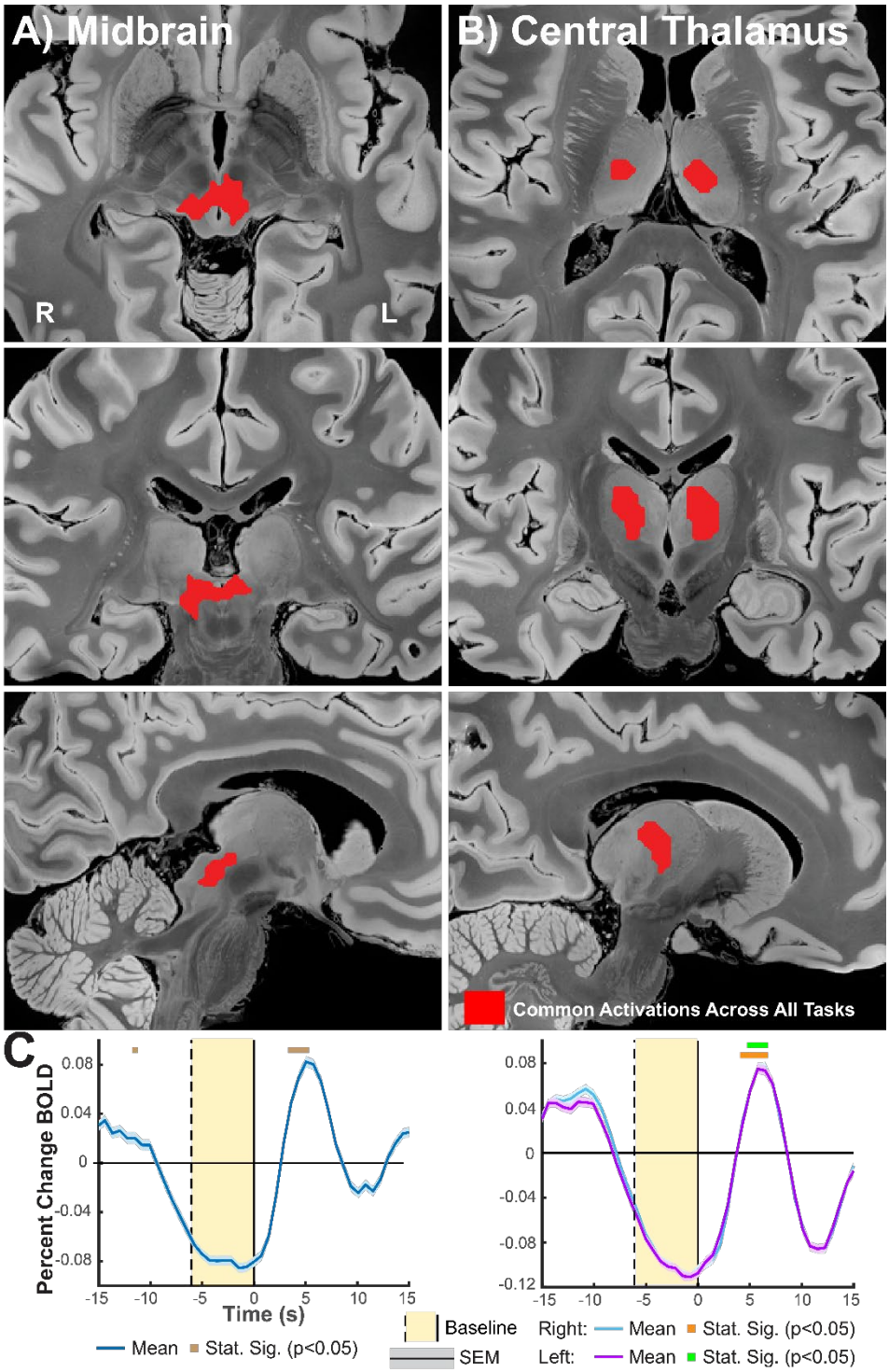
A) Midbrain
B) Central Thalamus
R
L
Common Activations Across All Tasks
C
Percent Change BOLD
0.08
0.04
0
-0.04
-0.08
-0.12
-15
-10
-5
0
5
10
15
Time (s)
Mean
Stat. Sig. (p<0.05)
Baseline
SEM
Right:
Left:

Figure 2:

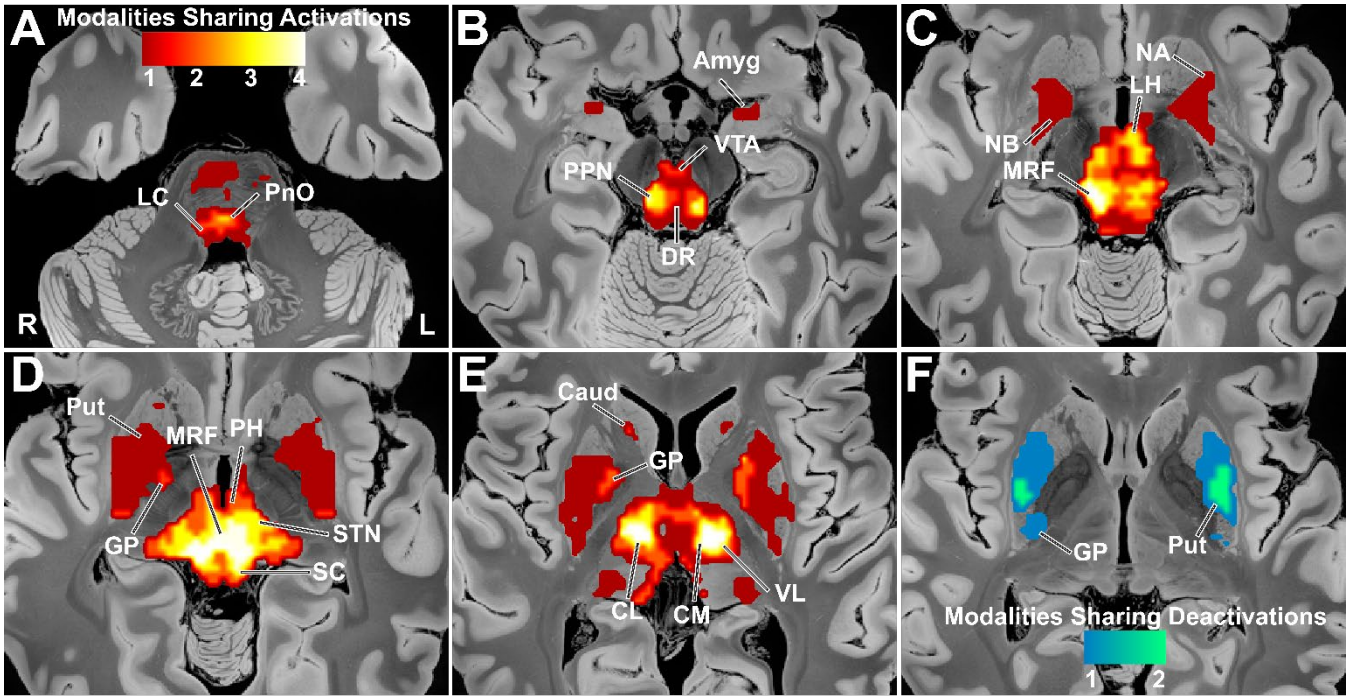
A
Modalities Sharing Activations
1 2 3 4
LC
PnO
R
L
B
Amyg
VTA
PPN
DR
C
NA
LH
NB
MRF
D
Put
MRF
PH
GP
STN
SC
E
Caud
GP
CL
CM
VL
F
GP
Put
Modalities Sharing Deactivations
1 2

Figure 3:

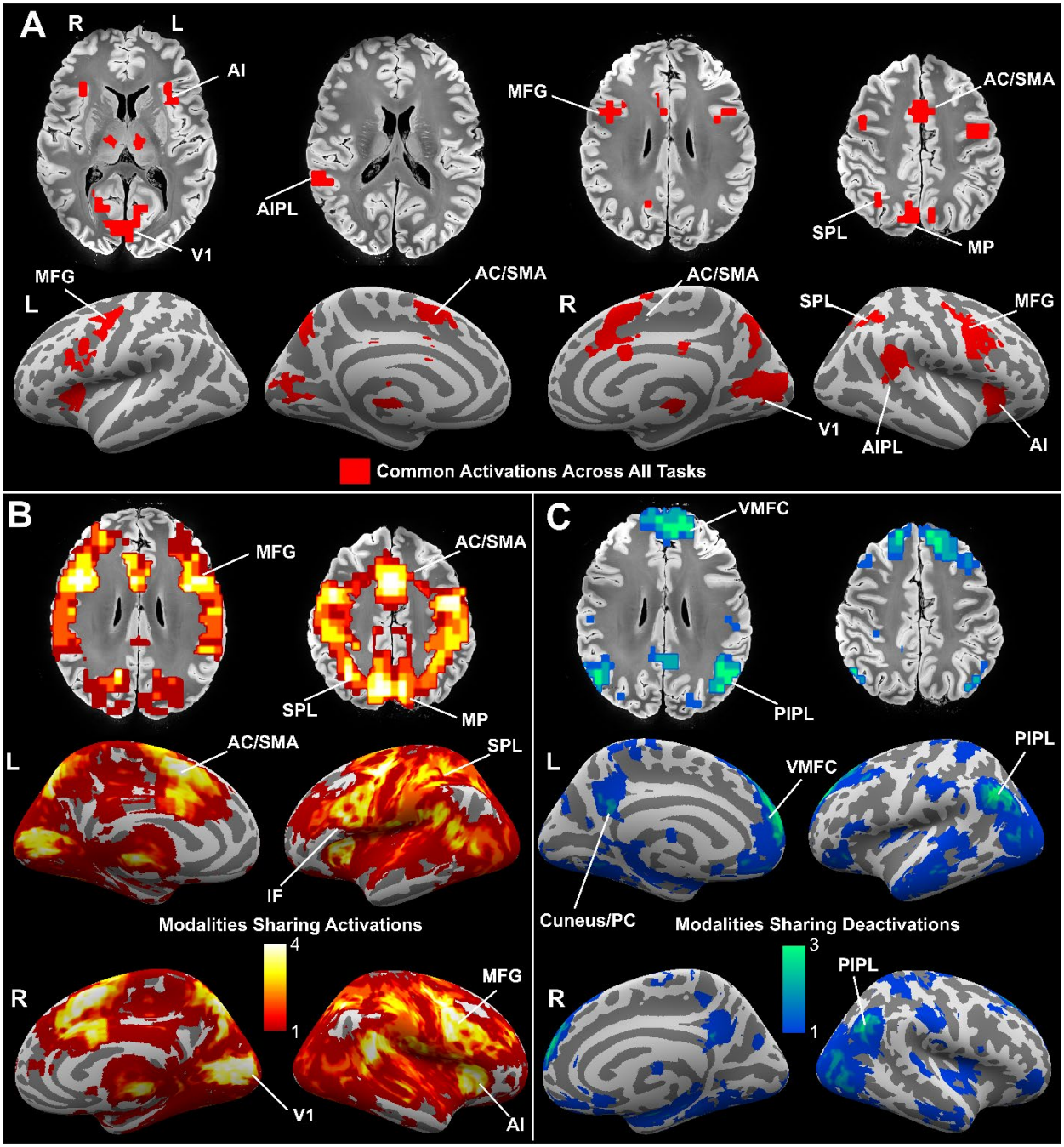
A
R
L
AI
AIPL
V1
MFG
AC/SMA
SPL
MP
L
R
Common Activations Across All Tasks
B
C
VMFC
PIPL
Cuneus/PC
IF
Modalities Sharing Activations
Modalities Sharing Deactivations
4
1
3

Figure 4:

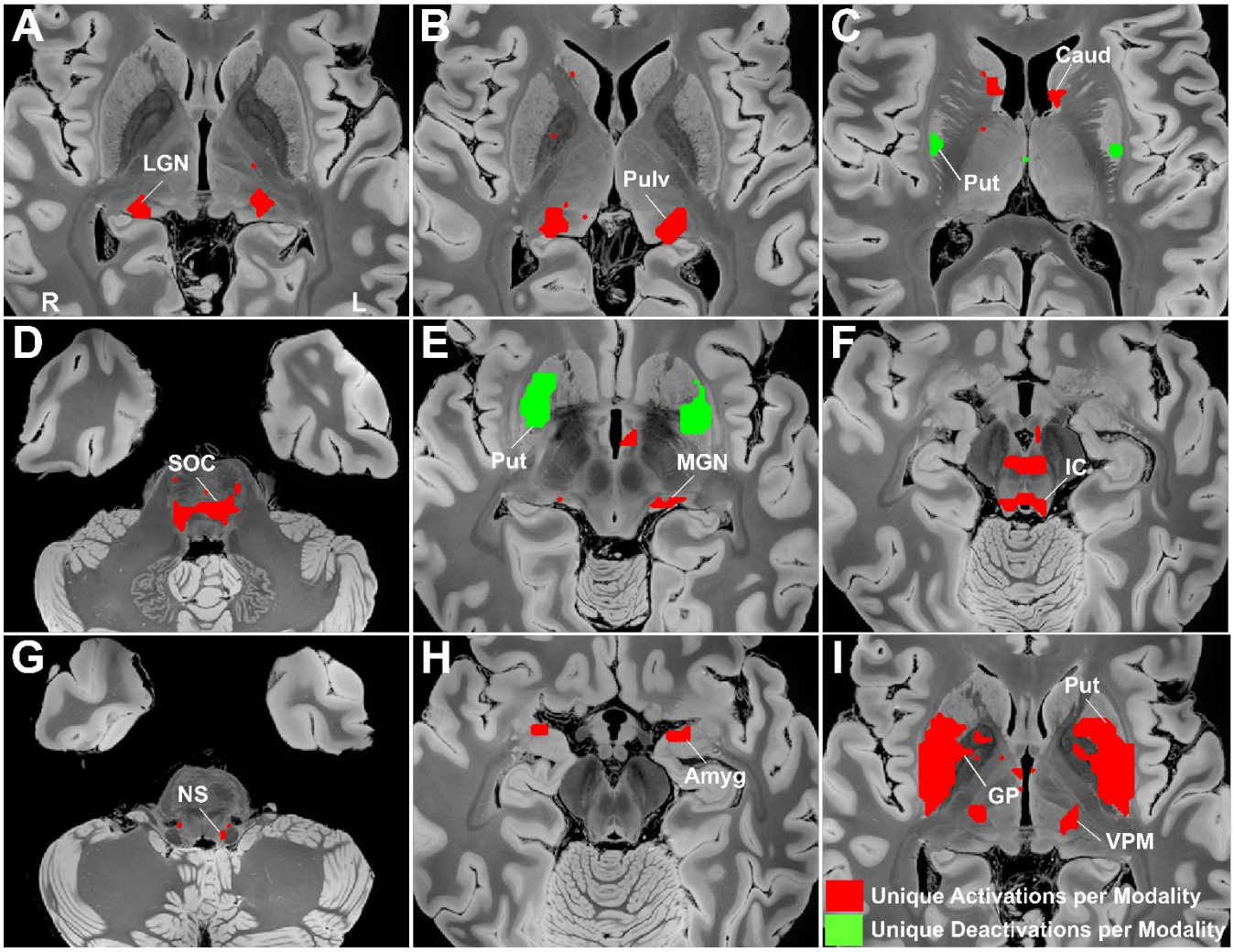
A
LGN
R
L
B
Pulv
C
Caud
Put
D
SOC
E
Put
MGN
F
IC
G
NS
H
Amyg
I
Put
GP
VPM
Unique Activations per Modality
Unique Deactivations per Modality

Figure 5:

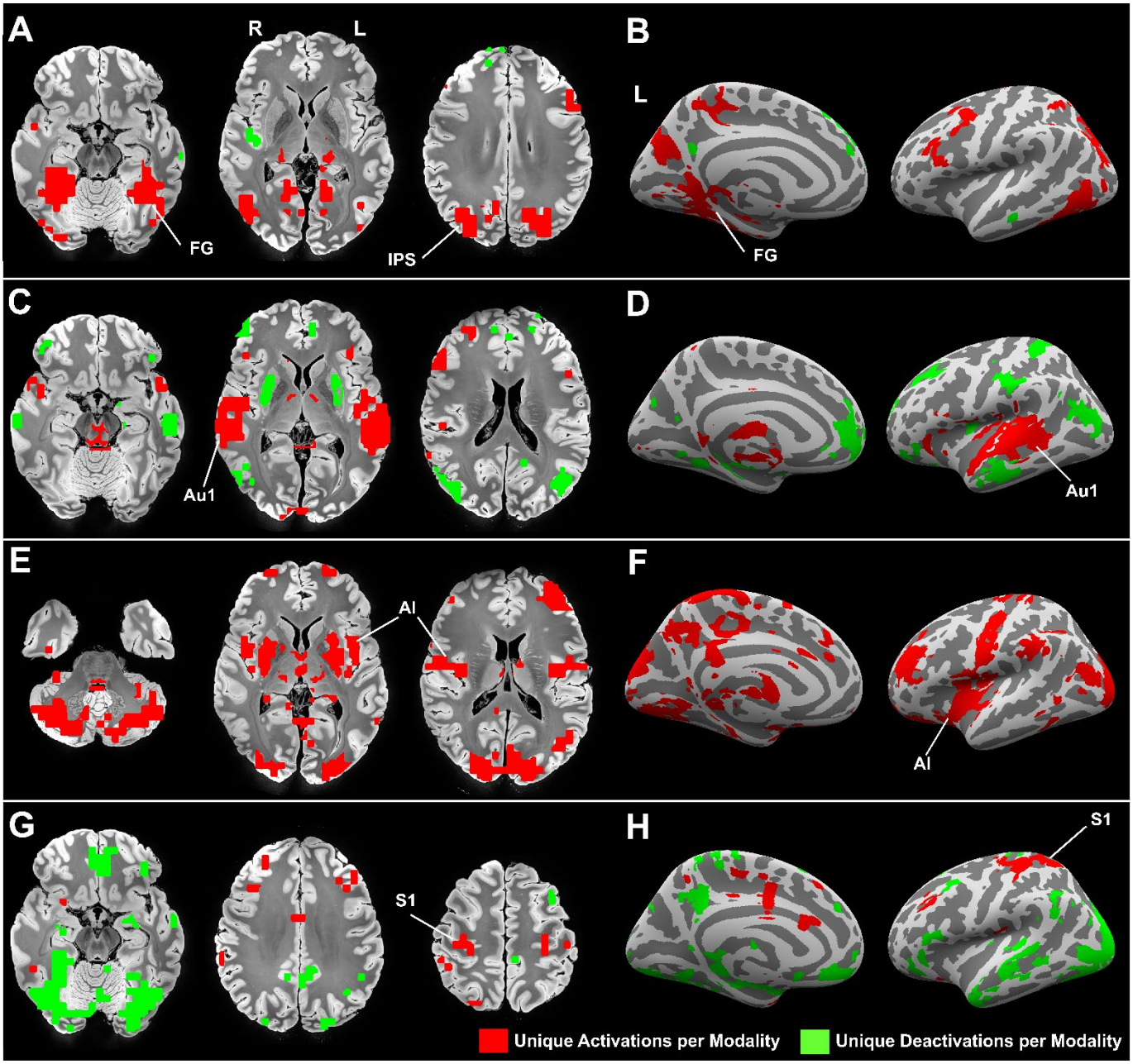
A
R
L
FG
IPS
B
L
FG
C
Au1
D
Au1
E
AI
F
AI
G
S1
H
S1
Unique Activations per Modality
Unique Deactivations per Modality

Table 1: Overview of the tasks employed in this study, including key design characteristics and analysis-relevant details.

Dataset	Task	Stimulus modality	Analysis type	Duration of task, rest blocks (s)	Blocks of task, rest per run	Number of runs, number of blocks or events analyzed per run	Participants
HCP	Gambling	Visual	Block	28, 15	4, 4	2, 3	1088
HCP	Relational Processing	Visual	Block	16, 16	6, 3	2, 2	1045
HCP	Working Memory	Visual	Block	25, 15	8, 4	2, 3	1091
HCP	Social Cognition	Visual	Block	23, 15	5, 5	2, 4	1054
HCP	Motor	Visual	Block	12, 15	10, 3	2, 2	1086
HCP	Language	Auditory	Event	28, NA	8, NA	2, 12-15[a]	1054
UCLA	Spatial Capacity	Visual	Event	NA, NA	NA, NA	2, 48	130
Glasgow	Passive Listening	Auditory	Block	8, 12	40, 20	1, 19	217
Yale	Taste Perception I	Taste	Block	36-72, 15	8, 8	4, 7	28
Yale	Taste Perception II	Taste	Block	36-72, 10	12, 12	2, 11	48
Jag. Univ.	Reading Braille	Tactile	Block	4-6, 4-8	72, 7	8, 0-2[b]	25

[a] Each run in the language task contains 4 story blocks and 4 math blocks. Each story block contained one story and each math block contained between 2-3 math problems yielding 12-15 events per run.

[b] Analysis of rest-tactile task transitions in the reading Braille task was conducted in 5 runs, each containing two blocks, and in 2 runs, each containing one block. One run had no analyzed blocks due to the lack of rest-tactile task transitions.

*NA: Not Applicable

Data are from the Human Connectome Project (HCP)[38, 39], University of California Los Angeles (UCLA) Consortium for Neuropsychiatric Phenomics[40], Glasgow University[41], Yale University[43, 44], and Jagiellonian University (Jag. Univ.)[42].

Table 2: Early transient BOLD fMRI changes in different subcortical ROIs across sensory modalities within four seconds from block/event onset.

		Increases or Decreases in Each Modality				Changes Across Modalities	
Region	**ROI**	**Visual (L, R)**	**Auditory (L, R)**	**Taste (L, R)**	**Tactile (L, R)**	**Shared Incr. (L, R)**	**Shared Decr. (L, R)**
Pons	Locus coeruleus	0,0	+,+	+,+	0,0	2,2	0,0
	Parabrachial nucleus	0,+	+,+	+,+	0,0	2,3	0,0
	Pontine nucleus oralis	0,+	+,+	+,+	0,0	2,3	0,0
Midbrain	Dorsal raphe	+	+	0	0	2	0
	Midbrain reticular formation	+,+	+,+	+,+	+,+	4,4	0,0
	Pedunculopontine tegmental nucleus	0,+	+,+	0,0	+,+	2,3	0,0
	Superior colliculi	+,+	+,+	+,+	+,0	4,3	0,0
	Ventral tegmental area	+	+	0	0	2	0
Hypothalamus	Lateral hypothalamus	+,+	+,0	+,0	0,0	3,1	0,0
	Posterior hypothalamus	+,+	+,0	+,+	0,0	3,2	0,0
Basal forebrain/	Amygdala	0,0	-,0	+,+	-,-	1,1	2,1
Amygdala	Nucleus Basalis	0,0	-,0	+,+	0,0	1,1	1,0
	Central lateral nucleus	+,+	+,+	+,+	+,+	4,4	0,0
	Centromedian nucleus	+,+	+,+	+,+	0,+	3,4	0,0
Thalamus	Mediodorsal nucleus	+,+	+,+	+,+	+,+	4,4	0,0
	Ventral lateral nucleus	+,+	+,+	+,+	+,+	4,4	0,0
	Ventral medial nucleus	+,+	+,+	+,+	0,+	3,4	0,0
	Caudate	0,+	0,0	0,0	+,+	1,2	0,0
Basal Ganglia	Putamen	0,0	-,-	+,+	-,-	1,1	2,2
	Globus pallidus	+,+	-,-	+,+	-,-	2,2	2,2
	Nucleus accumbens	0,0	0,0	0,0	0,+	0,1	0,0
	Subthalamic nucleus	+,+	+,+	+,+	0,0	3,3	0,0

In the first four columns, for each modality +, -, 0 denote statistically significant increases, decreases, or no change, respectively at four seconds after block/event onset in a given ROI. Changes are shown for left (L) and right (R) sides for bilateral ROIs. The dorsal raphe and ventral tegmental area were single midline ROIs without left or right sides, so only single values are shown for those two ROIs. The right two columns show total number of modalities with significant increases (Incr.) or decreases (Decr.) for each ROI.